

Shear measurement bias II: a fast machine learning calibration method

Arnau Pujol^{1,2,3,4}, Jerome Bobin^{1,2,5}, Florent Sureau^{1,2}, Axel Guinot^{1,2}, and Martin Kilbinger^{1,2,6}

¹ DEDIP/DAP, IRFU, CEA, Université Paris-Saclay, F-91191 Gif-sur-Yvette, France

² AIM, CEA, CNRS, Université Paris-Saclay, Université Paris Diderot, Sorbonne Paris Cité, F-91191 Gif-sur-Yvette, France

³ Institut d'Estudis Espacials de Catalunya (IEEC), E-08034 Barcelona, Spain

⁴ Institute of Space Sciences (ICE, CSIC), E-08193 Barcelona, Spain

⁵ Institute of Particle and Cosmos Physics (IPARCOS), Universidad Complutense de Madrid, E-28040 Madrid, Spain

⁶ Institut d'Astrophysique de Paris, UMR7095 CNRS, Université Pierre & Marie Curie, 98 bis boulevard Arago, F-75014 Paris, France

Received date / Accepted date

ABSTRACT

We present a new shear calibration method based on machine learning. The method estimates the individual shear responses of the objects from the combination of several measured properties on the images using supervised learning. The supervised learning uses the true individual shear responses obtained from copies of the image simulations with different shear values. On simulated GREAT3 data, we obtain a residual bias after the calibration compatible with 0 and beyond Euclid requirements for $\text{SNR} > 20$ within ~ 15 CPU hours of training using only $\sim 10^5$ objects. This efficient machine learning approach can use a smaller data set since the method avoids the contribution from shape noise. Also, the low dimensionality of the input data leads to simple neural network architectures. We compare it to the state-of-the-art method Metacalibration, showing similar performances, and their different methodologies and systematics suggest them to be very good complementary methods. Our method could therefore be fastly applied to any survey such as Euclid or LSST, with less than a million images to simulate to learn the calibration function.

Key words. weak gravitational lensing - shear bias - machine learning

1. Introduction

Weak gravitational lensing by the large-scale structure has become an important tool for cosmology in recent years. Light deflection by tidal fields of the inhomogeneous matter on very large scales cause small deformations of images of high-redshift galaxies. This cosmic shear contains valuable information about the growth of structures in the universe, and can help to shed light on the nature of dark matter and dark energy. The amount of shear that is induced by weak lensing is very small, at the percent-level, and should be estimated from galaxy images with a high accuracy for reliable cosmological inference: measurement biases need to be reduced to the sub-percent level to pass the requirement of upcoming large cosmic-shear experiments, such as the ESA space mission Euclid (Laureijs et al. 2011), the NASA space satellite WFIRST (Akeson et al. 2019), or the ground-based telescope LSST (LSST Science Collaboration et al. 2009).

Shear is estimated by measuring galaxy shapes, and averaging out their intrinsic ellipticity. This estimate is in general biased, due to noise, inappropriate assumptions about

the galaxy light distribution, uncorrected PSF residuals, and detector effects such as the brighter-fatter effect or charge transfer inefficiency (Bridle et al. 2009, 2010; Kitching et al. 2010, 2012, 2013; Refregier et al. 2012; Kacprzak et al. 2012; Melchior & Viola 2012; Taylor & Kitching 2016; Massey et al. 2007, 2013; Voigt & Bridle 2010; Bernstein 2010; Zhang & Komatsu 2011; Kacprzak et al. 2012, 2014; Mandelbaum et al. 2015; Clampitt et al. 2017). The resulting shear biases are complex functions of many parameters, which describe galaxy and instrument properties. These include the galaxy size, flux, morphology, signal-to-noise-ratio, intrinsic ellipticity, PSF size, anisotropy and its alignment with respect to the galaxy orientation, and many more (Zuntz et al. 2013; Fenech Conti et al. 2017; Hoekstra et al. 2015, 2017; Pujol et al. 2017).

To achieve the sub-percent shear bias expected in future cosmic-shear surveys, the shear estimates typically need to be calibrated using a very high number of simulated images to overcome for instance the statistical variability induced by galaxy intrinsic shapes (Massey et al. 2013). Furthermore, these simulations need to span adequately the high-

dimensional space of parameters that determine the shear bias. Otherwise, regions of parameter space that are under-represented in the simulations compared to the observations can lead to incorrect bias correction. The selection of objects needs to closely match the real selection function, to avoid selection biases.

Existing calibration methods requiring extensive image simulations select a priori a few parameters of interest, often galaxy size and SNR, for which the shear bias variation is estimated (Zuntz et al. 2018). The shear bias is computed using various methods such as fitting to the parameters (Jarvis et al. 2016; Mandelbaum et al. 2018b) or k -nearest neighbours (Hildebrandt et al. 2017).

Machine learning techniques have been employed as well for shear estimation and calibration. Gruen et al. (2010) train an artificial neural network (NN) to minimize the shear bias from parameters measured in the moment-based method KSB (Kaiser et al. 1995). More recently, Tewes et al. (2019) present an artificial neural network for supervised learning, to obtain shear estimates from a few fitted parameters from images using adaptive weighted moments via regression and using as training set image simulations with varying galaxy features.

An alternative shear calibration method that does not require image simulations and is based on the data themselves is the so-called meta-calibration (Huff & Mandelbaum 2017). This approach computes the shear response matrix by adding small shear values to deconvolved observed galaxy images. A hybrid method is a self-calibration (Fenech Conti et al. 2017), for which noise-free simulated images are created and re-measured, according to the best-fit parameters measured on the data, to reduce noise bias.

This paper extends previous work of machine learning for shear calibration. In the companion paper Pujol et al. (2017), hereafter Paper I, we have explored the dependence of shear bias for various combinations of input and measured parameters. We demonstrated the complexity of this shear bias function, and showed the importance to account for correlations between parameters. A multi-dimensional parameter space of galaxy and PSF properties is therefore set up to learn the shear bias function using a deep learning architecture to regress the shear bias from these parameters.

This paper is organized as follows. Sect. 2 presents the definition of shear bias, and review our methodology to measure shear bias introduced in Pujol et al. (2019) (hereafter PKSB19). In Sect. 3 we introduce our new shear calibration method. Sect. 4 presents the simulated images and the input data used for the training, test and validation of our method to produce the results of this paper, which are discussed and compared to an existing method in Sect. 5. After a discussion of several points regarding the new method in Sect. 6 we conclude with a summary of the study in Sect. 7.

2. Shear bias

2.1. Shear bias definition

In the weak-lensing regime, the observed ellipticity of a galaxy e_i^{obs} is an estimator of the reduced shear g_i , for com-

ponent $i = 1, 2$. In general however, this estimator is biased due to pixel noise, PSF residuals, inaccurate galaxy models and other effects (see Mandelbaum (2018) for a recent review). The bias of the estimated shear, g^{obs} , is usually expressed by the following equation:

$$\langle e_i^{\text{obs}} \rangle = g_i^{\text{obs}} = c_i + (1 + m_i)g_i, \quad (1)$$

where c_i, m_i are the additive and multiplicative shear biases, respectively. For a constant shear, if the mean intrinsic ellipticity of a galaxy sample is zero we can measure the shear from the average observed ellipticities using the above relation.

We can also define the response of the ellipticity measurement of an image to linear changes in the shear (Huff & Mandelbaum 2017):

$$R_{ij} = \frac{\partial e_i^{\text{obs}}}{\partial g_j}. \quad (2)$$

The multiplicative bias of a population can be obtained from the average shear responses, as described in Pujol et al. (2019):

$$1 + m_i = \langle R_{ii} \rangle. \quad (3)$$

In a similar way, the additive population shear bias can be obtained from the average of the individual additive biases:

$$c_i = \langle e_i^{\text{obs}} - e_i^{\text{I}} - R_{ii}g_i \rangle = \langle e_i^{\text{obs}} \rangle, \quad (4)$$

where e_i^{I} is the intrinsic ellipticity, and the second equality holds if $\langle e_i^{\text{I}} \rangle = 0$ and $\langle R_{ii}g_i \rangle = 0$ (which is true if R_{ii} is not correlated with g_i and $\langle g_i \rangle = 0$).

2.2. Shear bias measurements

In this paper we use two methods to estimate shear bias, both of which we briefly describe in this section. For more details on the different methods to estimate shear bias in simulations we refer the reader to PKSB19.

First, to test the residual shear bias after calibration, we use the common approach to measure shear bias from a linear fit to eq. (1). We simulate each galaxy with its orthogonal pair to guarantee the average intrinsic ellipticity to be zero. This improves the precision of the shear bias estimation by a factor of ~ 3 , as shown in PKSB19.

Second, to study the shear bias dependencies, we use the method introduced in PKSB19: We measure the individual shear responses and additive biases from each galaxy image by using different sheared versions of the same image. The multiplicative and additive bias of a population is then obtained from the average of these quantities. This method has been proven to be more precise by a factor of ~ 12 compared to the linear fit with orthogonal-pair noise cancellation (PKSB19).

These individual shear responses and additive biases are also used as quantities for the supervised machine-learning algorithm of our calibration method (Sect. 3.2). We will denote the biases measured from simulations as described here as ‘true’ biases m_i^t, c_i^t , indicated with the superscript ‘t’. Our goal in this paper is to regress these biases in a high dimensional parameter space where this function is living.

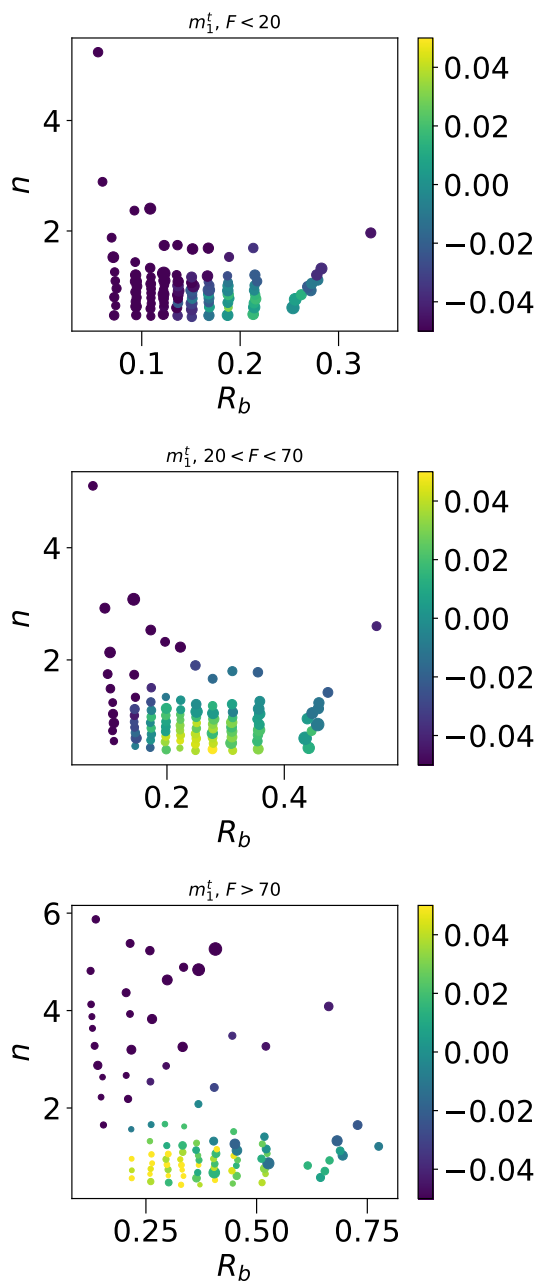


Fig. 1. Color-coded true multiplicative shear bias m_1^t as a function of input galaxy properties. The y -axis shows the Sérsic index n , the x -axis is the half-light radius R_b . The top, middle and bottom panels show galaxies with different fluxes, corresponding to $F < 20$, $20 < F < 70$ and $F > 70$, respectively. Each point is to the mean over an equal number of galaxies, the point size is inversely proportional to the error bar, such that large points are more significant.

2.3. Dependencies

Shear bias depends in a complex way on various properties of the observed galaxy and image properties. In Paper I we explore some of these dependencies using the same simulated GREAT3 images as in this paper.

In Fig. 1 we show an example of shear bias dependencies with respect to three galaxy properties. In each panel we see that the multiplicative bias m_1 depends on both the Sérsic index n and the half-light radius R_b . In addition, these dependencies change with the galaxy flux F (the three panels show increasing ranges of flux from top to bottom). We therefore need to know all three quantities to constrain m_1 , and its dependence on n , R_b , and F cannot be separated. This is just one example, but it illustrates the general, very complex functional form of shear bias with respect to many galaxy properties. For shear calibration of upcoming high-precision surveys, this sets very high demands on image simulations, which need to densely sample a high-dimensional parameter space of galaxy and image properties.

3. Deep-learning shear calibration

3.1. Why machine learning for shear calibration?

Sect. 2.3 and Paper I gave a glimpse of shear bias as a very complex, non-linear function acting on a high-dimensional parameter space of galaxy and image properties. For a successful shear calibration to sub-percent residual biases required for large upcoming surveys (e.g. Massey et al. 2013), this function needs to be modeled very accurately. This is true whether the calibration is performed galaxy by galaxy, or globally by forming the mean over an entire galaxy population: shear bias measured on simulations is always marginalized over some unaccounted parameters, explicitly or implicitly. If shear bias depends on some of the unaccounted parameters, then the mean bias will be sensitive to the distribution of these parameters over the population used, and a mismatch of this distribution between simulations and observations will produce a wrong shear bias estimation and calibration. For this reason it is crucial to model shear bias as a function of a wide range of properties to minimize the impact of the remaining unaccounted parameters. With this we would still not have control of the shear bias dependence on the distribution over remaining unaccounted parameters, but we would have already captured the most significant dependencies. Generating a sufficiently large number of image simulations in this high-dimensional, non-separable space, obviously sets enormous requirements on computation time and storage for shear calibration.

The exact form of the shear bias function is not interesting per se. In addition, it is very difficult to determine this function from first principles, based on physical considerations (Refregier et al. 2012; Taylor & Kitching 2016; Hall & Taylor 2017; Tessore & Bridle 2019). In general, for most simulation-based calibration methods empirical functions are fitted. However, we can make a few, very basic and general assumptions about this function. For example, galaxies with similar properties are expected to have a similar shear bias under a given shape measurement method. Further, this function is expected to be smooth (with a possible stochasticity coming from noise). These basic properties makes the shear bias function ideal to be obtained with machine-learning (ML) techniques.

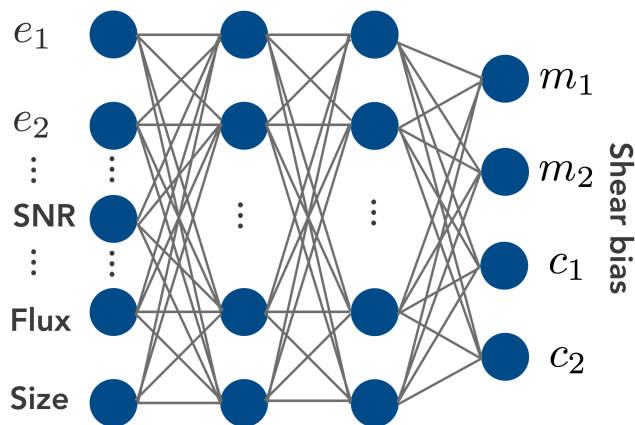


Fig. 2. Visual schema of the machine learning approach of the method.

The problem of estimating the shear bias from galaxy image parameters requires to finely capture the dependencies described above. On the one hand, and from a mathematical point of view, the smoothness of the relationship between shear bias and parameters tells us that shear bias should belong to a smooth low-dimensional manifold. Estimating such a manifold structure then boils down to some regression problem. On the other hand, the relationship between the measured parameters and the sought-after shear is very intricate, which impedes the use of standard regression methods, but for which machine-learning methods are very well suited.

ML can account for many parameters, and model a very complex, high-dimensional function of shear bias. The dependence on unaccounted parameters of the marginalized shear bias is expected to be small, and the calibration becomes less sensitive to the particular population that is simulated. If properly designed, we do not need to know beforehand the exact important properties that affect shear bias, since the algorithm can learn what are the important combination of parameters to constrain shear bias. One still needs to know the distribution of properties of observed galaxies, which are noisy and might be biased. However, as we will see below, the ML training set can be different from the test set to some extent, with only relatively small calibration bias, see also discussion in Sect. 6.2.

3.2. Neural Network Shear Correction

In this section we describe our new method based on ML that we call Neural Network Shear Correction (NNSC). We describe the concepts of the ML approach, the learning and the calibration steps. We have made the code publicly available¹.

3.2.1. Concept

In the present article, the objective of the ML is to infer an estimate of the shear bias from a large number of galaxy image measurement parameters. To that end, a Deep Neural Network (DNN), and more precisely a multilayer feed-forward neural network, is particularly well adapted for tackling the underlying regression problem.

More precisely, a feed-forward neural network is composed of L layers, taking measured image properties as inputs and providing the shear bias as output. The resulting network aims at mapping the relationship between the measured properties of the galaxy images and the shear bias. The parameters of the network are then learnt in a supervised manner by minimizing the residual between the true and the estimated shear bias. The shear bias is estimated individually for each galaxy given their measured properties.

If x_i denotes a vector containing m measured properties $x_i[j]$ for $j = 1, \dots, m$ for a single galaxy i , then the output of the first layer $\ell = 1$ of the neural network is defined by some vector $h_j^{(1)}$ of size m_1 :

$$h_i^{(1)} = \mathcal{A} \left(\mathbf{W}^{(1)} x_i + b^{(1)} \right), \quad (5)$$

where $\mathbf{W}^{(1)}$ (*resp.* $b^{(1)}$) stands for the weight matrix (*resp.* the bias vector) at layer $\ell = 1$, x_i is the vector of the galaxy with index i and j is the index referring to a measured property. The term \mathcal{A} is the so-called activation function, which applies entry-wise on its argument. For a layer $\ell = n$, the output vector of size m_n is defined as:

$$h_i^{(n)} = \mathcal{A} \left(\mathbf{W}^{(n)} h_i^{(n-1)} + b^{(n)} \right). \quad (6)$$

For $\ell = 5$, the output vector $h_j^{(L)}$ stands for the estimated shear bias components. A visual schema of the method is shown in Fig. 2.

3.2.2. Learning

The learning stage amounts to estimating the parameters $\{\mathbf{W}^{(\ell)}, b^{(\ell)}\}_{\ell=1, \dots, L}$ by minimizing the following cost function defined as some distance (the χ^2) between the shear bias components and their estimates:

$$C = \frac{1}{b_s} \sum_{i=0}^{b_s} \sum_{\alpha=1}^2 (m_{i,\alpha}^t - m_{i,\alpha}^e)^2 + (c_{i,\alpha}^t - c_{i,\alpha}^e)^2, \quad (7)$$

where m_{α}^t , c_{α}^t and m_{α}^e , c_{α}^e are the true and estimated α th component of the shear multiplicative and additive bias, respectively, and b_s is the number of objects used in each training step (also referred as batch size). We use as true shear bias the values from equations (2) and (4) obtained as described in Sect. 2 and presented in Pujol et al. (2019). The NNSC learns to estimate these shear biases.

¹ <https://github.com/arnaupujol/nnsc>

We use $m = 27$ measured properties used as input for the model as described in Sect. 4.2, and details about the network architecture and the implementation of the learning stage are given in Appendix A.

3.2.3. Calibration

The NNSC method estimates the shear responses and biases of individual galaxies from the measurements of 27 properties applied to the images. Notice that the shear bias and the corresponding calibration are done for a previously chosen shape measurement. Any shape measurement algorithm can be chosen for this purpose, in our case we use the estimation from the KSB method using the software SHAPELENS. Once these estimations are done we can apply the shear calibration over the statistics of interest, in our case the estimated shear from Eq. 1. The bias calibration is applied as $\langle \mathbf{R} \rangle^{-1} \langle e^{\text{obs}} - \langle \mathbf{c} \rangle \rangle$, where \mathbf{R} and \mathbf{c} are the estimated average shear response and additive bias respectively (see Sheldon & Huff 2017).

Our method gives estimates for the individual shear bias of objects, in common with the state-of-the-art method METACALIBRATION. However, the two methods are very different. While NNSC relies on image simulations for a supervised machine learning approach, METACALIBRATION uses the data images themselves to obtain the individual shear responses. To do this, the original data images are deconvolved with an estimated PSF and, after applying some shear, they are re-convolved with a slightly larger PSF. Because this method is very complementary with respect to NNSC and it has been recently used in surveys such as the Dark Energy Survey (DES) (Zuntz et al. 2018), we use it in this study for a calibration comparison of both models. For more details about METACALIBRATION we refer to a description of the implementation in the Appendix B and the original papers (Huff & Mandelbaum 2017; Sheldon & Huff 2017).

4. Data

4.1. Image simulations

We consider in this work two sets of GALSIM simulations (Rowe et al. 2015), corresponding essentially to the control-space-constant (CSC) and real-space-constant (RSC) branch simulated in GREAT3 (Mandelbaum et al. 2014), with some modifications to ensure precise measurement of the shear response as prescribed in PKSB19.

The CSC branch contains galaxies with parametric profiles (either a single Sérsic or a de Vaucouleurs bulge profile with and exponential disk added) obtained from fits to HST data from the COSMOS survey with realistic selection criteria (Mandelbaum et al. 2014). This data set intended to provide realistic distribution of galaxy properties (in particular in terms of morphology, size, signal to noise ratio), which we could therefore use to train and test our calibration network with.

As for GREAT3, the 2 million galaxy images are divided into 200 images of 10000 galaxies, each one with a

different pre-defined shear and point spread function (PSF) applied. Each galaxy is randomly oriented, and its orthogonal version is included as well in the dataset to allow for nulling the average intrinsic ellipticity. Out of these 200 images, we select a first set for training and a second set for testing and comparing calibration approaches. For the training set, we follow the approach of PKSB19 described above to obtain an estimate of the true shear response that need to be learnt. For each galaxy in the training set, five sheared versions are simulated keeping PSF and noise realizations the same. The shear \mathbf{g} for each galaxy was chosen as $\mathbf{g}_i = \{(g_1, g_2)_i\} = \{(0, 0), (\pm 0.02, 0), (0, \pm 0.02)\}$.

To further investigate the impact of model bias in our procedure, the network predictions are tested as well for more realistic galaxies simulated as in the RSC branch of GREAT3. These galaxies are based on actual observations from the HST COSMOS survey, fully deconvolved with the HST PSF (see procedure in Mandelbaum et al. (2013)), prior to applying random rotation, translation, and the prescribed shear followed by convolution with the target PSF and resampling in the target grid. In this scenario, the same procedure as for CSC is followed to obtain estimates of the shear response for these realistic galaxies, which can then be compared to the network predictions based on the CSC training set.

4.2. Learning input data

The image properties used for the shear bias estimation can be chosen depending on the interest. The NNSC will learn to estimate shear bias as a function these properties, so the more properties we use the more capable the NNSC will be to learn complex dependencies (if we use the appropriate training).

In this paper we use 27 measured properties as input for the NNSC. These properties correspond to the output from GFIT (properties such as ellipticities, fluxes, sizes, fitted disk fraction and other fitting statistics), the SHAPELENS KSB implementation (ellipticities, SNR and the size of window function used) and SEXTRACTOR (properties such as flux, size, SNR, and magnitude from both the galaxy and the PSF). We refer to Paper I for the details on the algorithms and implementations and to Table 1 for the list of measured properties used for the training.

In the following we report the results obtained with the network selected as described in Appendix A associated with the superscript "fid", referring to the fiducial implementation of the method.

5. Results

5.1. Bias predictions

In Fig. 3 we show the distribution between estimated and true shear biases in the validation set of the CSC branch. We show m_1 (top panel) and c_1 (bottom panel), but similar results are found for m_2 and c_2 . We see that the estimated and true biases are correlated, although the relation is scattered. We also see that the distribution of values is narrower

GFIT	SEXTRACTOR	KSB
Galaxy ellipticity $e_{1,\text{GFIT}}, e_{2,\text{GFIT}}$	Galaxy flux F_{out}	Ellipticity $e_{1,\text{KSB}}, e_{2,\text{KSB}}$
Axis ratio	Galaxy size	Ellipticity wrt to PSF $e_{+,\text{KSB}}, e_{\times,\text{KSB}}$
Orientation angle	SNR _{obs}	Axis ratio q_{KSB}
Galaxy flux	Galaxy magnitude	Orientation angle β_{KSB}
Disk radius	PSF flux	Window function size
Bulge radius	PSF size	SNR
Disk fraction	PSF SNR	
Number of χ^2 evaluations	PSF magnitude	
Noise level	PSF FWHM	

Table 1. Measured properties used for the training process of NNSC.

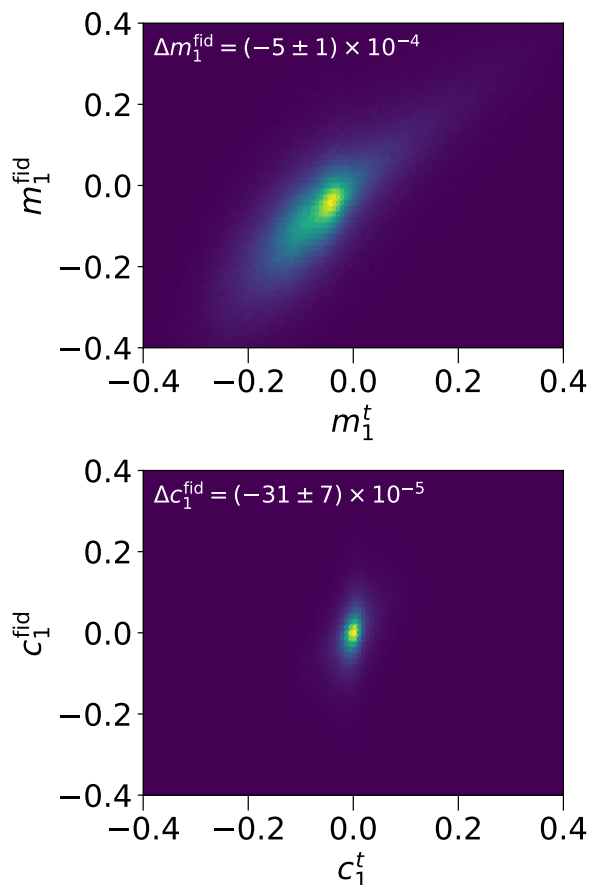


Fig. 3. Comparison between true and estimated shear bias. The multiplicative shear bias m_1 is shown in the top panel, and in the bottom panel we show the additive bias c_1 .

for the estimated biases than for the true. This is because the estimated bias is a function of the measured parameters with no noise stochasticity. It has been learned from the stochastic true values that are affected by noise, but the estimated function is not stochastic.

The errors on the estimated average biases are $\Delta m_1 = (4.9 \pm 1.1) \times 10^{-4}$ and $\Delta c_1 = (-3.1 \pm 0.7) \times 10^{-4}$ (similar values are found for the second components, with $\Delta m_2 = (0.0 \pm 1.1) \times 10^{-4}$ and $\Delta c_2 = (1.6 \pm 0.7) \times 10^{-4}$). These values are well below the Euclid requirements ($\Delta m < 2 \times 10^{-3}$

and $\Delta c < 5 \times 10^{-4}$), although a proper test on Euclid simulations should be done to quantify the performance for this mission. Notice, however, that this performance is obtained using only 128,000 objects with a ~ 15 CPU hours of training.

To obtain this precision we used a validation set of around 1,800,000 objects. According to the results from PKS19, we would expect an error on the mean bias of $\sim 3 \times 10^{-4}$. However, here we show the error on $m_1^t - m_1^{\text{est}}$. If these two quantities are correlated (as they are), the error on their difference can be smaller, as we show.

5.2. 1d dependencies

In Fig. 4 we show some examples of shear bias dependencies for different cases. In black we show the true multiplicative bias obtained as described in Sect. 2.2 that has been used for the supervised training. The dark red line corresponds to the performance of the NNSC estimation, referred as m^{fid} since it represents the fiducial training parameterization used for this paper (for other parameterizations see Appendix A). In the left panels we show dependencies on input simulation parameters. These are parameters that have been used to generate the image simulations with GALSIM, but they have not been used for NNSC. So, the training has not access to these properties. In the right panels we show dependencies on measured parameters that have been used for the training. The top panels show the m dependence on galaxy flux, and the bottom panels on SNR. The excellent performance on the right panels shows that the training correctly reproduces the dependencies on the measured parameters used as the training input. The left panels show that, although the performance is not perfect, the measured parameters used in NNSC capture enough information to reproduce the dependencies with a good precision.

5.3. 2d dependencies

Fig. 5 shows examples of the multiplicative shear bias 2d-dependencies. Here the multiplicative bias m_1 is represented in colour, the left panels show the true bias and the right panels the estimations from NNSC. In this case, the top four panels show the dependencies as a function of input simulation parameters (not accessible for NNSC), and the bottom panels show the dependencies on measured

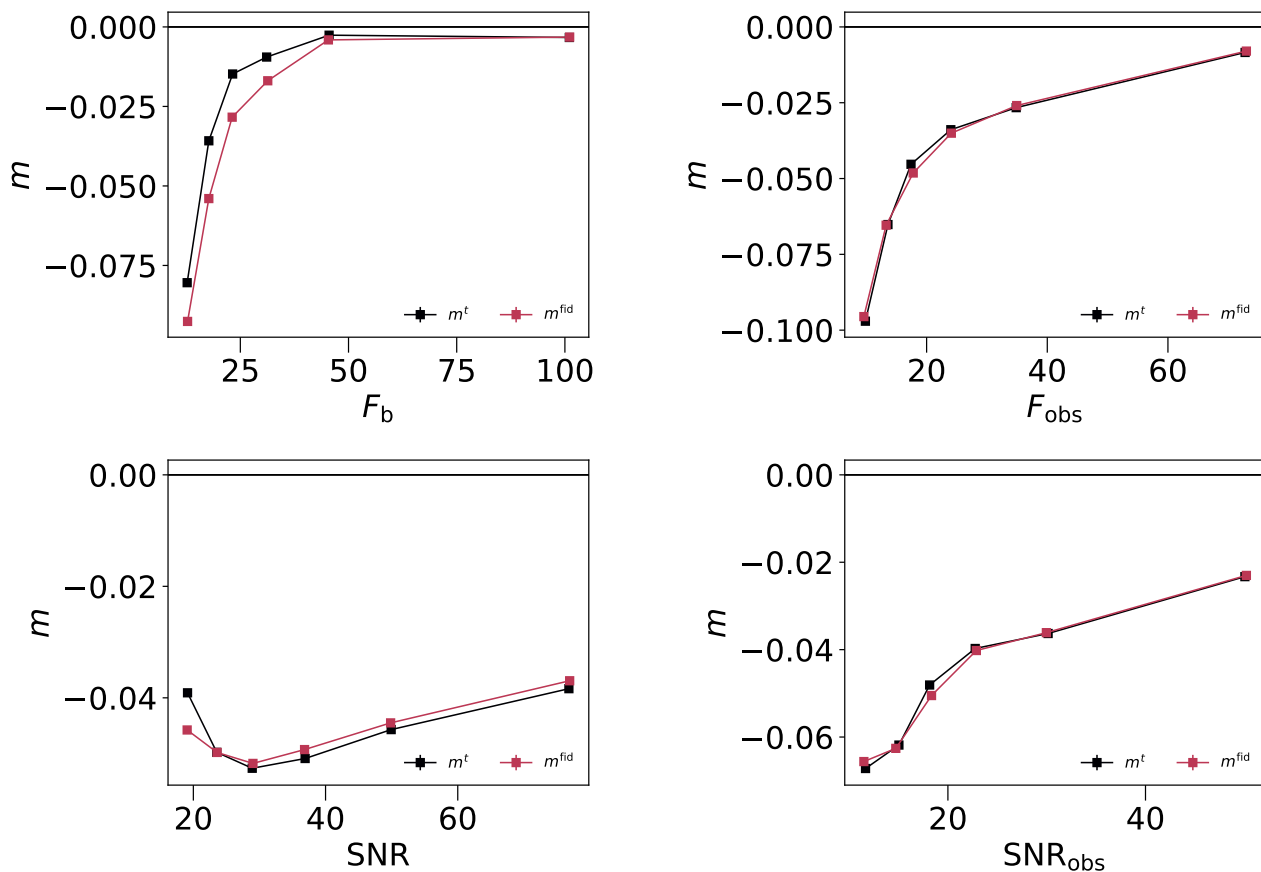


Fig. 4. Comparison of estimated versus true multiplicative shear bias m_1 as a function of several properties. Top panels show m as a function of galaxy flux, and bottom panels show m as a function of SNR. Left panels show input simulation properties from the galsim parameters, while right panels show measured parameters from SExtractor and used as inputs in the training of the NN.

parameters used for the training. We can see that NNSC gives a good prediction of shear bias as a function of combinations of two input properties. As before, the method is trained to describe shear bias as a function of the measured properties, in consistency with the good performance on the bottom panels, but the predictions on the input simulation parameters will depend on how much these properties are constrained by the measured parameters. We can see here that the method performs very well describing shear bias as a function of shape parameters (middle panels), but it underestimates the values for some galaxies with a very low Sérsic index n and intermediate radius. This is due to the fact that n has not been estimated and no properties referring to this parameter have been used for the training. The performance of the model would improve by using more measured properties on the training that are correlated with n (for example, a fitting parameter estimation of the galaxy profile).

5.4. Residual bias

In order to test the performance of the shear calibrations, we analyze the residual bias estimated from a linear fit of

Eq. 1 once the galaxy samples are corrected for their bias. Here we include METACALIBRATION as a reference for a state-of-the-art shear calibration method so that we can compare our performance with currently used approaches. With this we do not aim to show a competitive comparison between the methods, but to confirm the consistency of NNSC with respect to what can be expected for a solid method. The two methods are intrinsically different and affected by different systematics, so a combination of both methods can be a very complementary and robust approach for scientific analyses. Moreover, the two methods can be differently optimized for the performance in different types of data, and here we do not pretend to show the best case scenario for any of them. For details on the implementation done for METACALIBRATION see Appendix B.

In Fig. 6 we show the residual multiplicative bias m as a function of several input properties found for three different approaches. In black, the calibration has been done using the true shear bias obtained from the image simulations. This represents the best case scenario where the shear bias has been perfectly estimated and gives an estimation of the statistical uncertainty of the measurement. Red and cyan

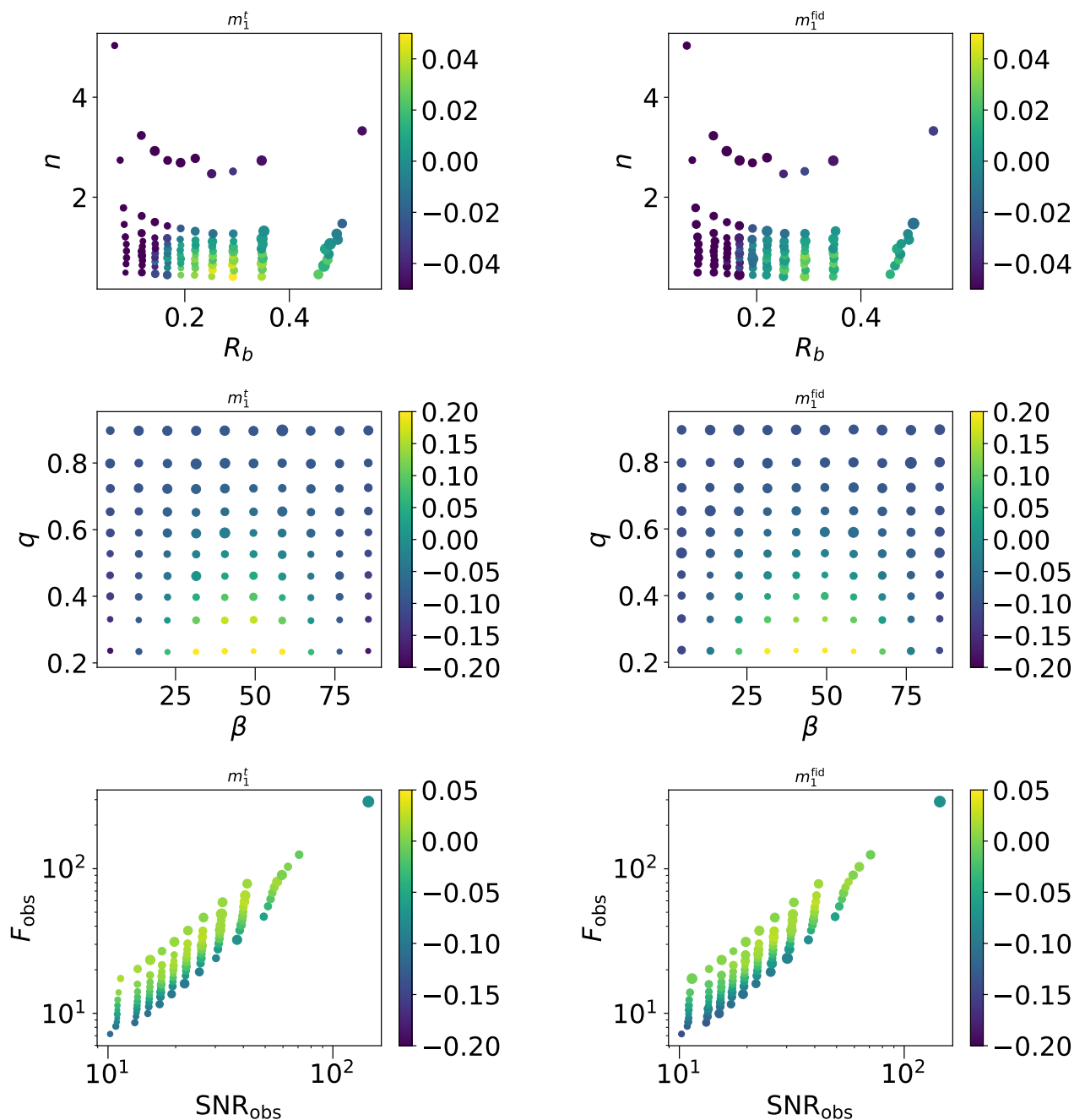


Fig. 5. Comparison of true (left panels) and estimated (right panels) multiplicative shear bias m_1 as a function of two properties simultaneously. Multiplicative shear bias is represented in colours. Each point is to the mean over an equal number of galaxies, and the point size is inversely proportional to the error bar, so that large points are more significant. Top panels: dependencies on Sérsic index n and bulge half-light radius from the simulation. Middle panels: dependencies on intrinsic ellipticity modulus q and orientation angle β from the simulation. Bottom panels: dependencies on the measured flux and SNR from SExtractor.

lines show the residual biases from METACALIBRATION and NNSC respectively.

We see that both methods show a residual bias below 1 for most of the cases, and the performance depends of the galaxy populations. In general, very good performances are found for both methods for bright or large galaxies. In

the case of METACALIBRATION, the residual multiplicative bias increases up to ~ 2 percent for small and dim galaxies, showing that the sensitivity of the method depends on the signal of the image, as expected. For NNSC, the performance depends on the property explored, going from negligible residual bias for any SNR, to a residual bias of up

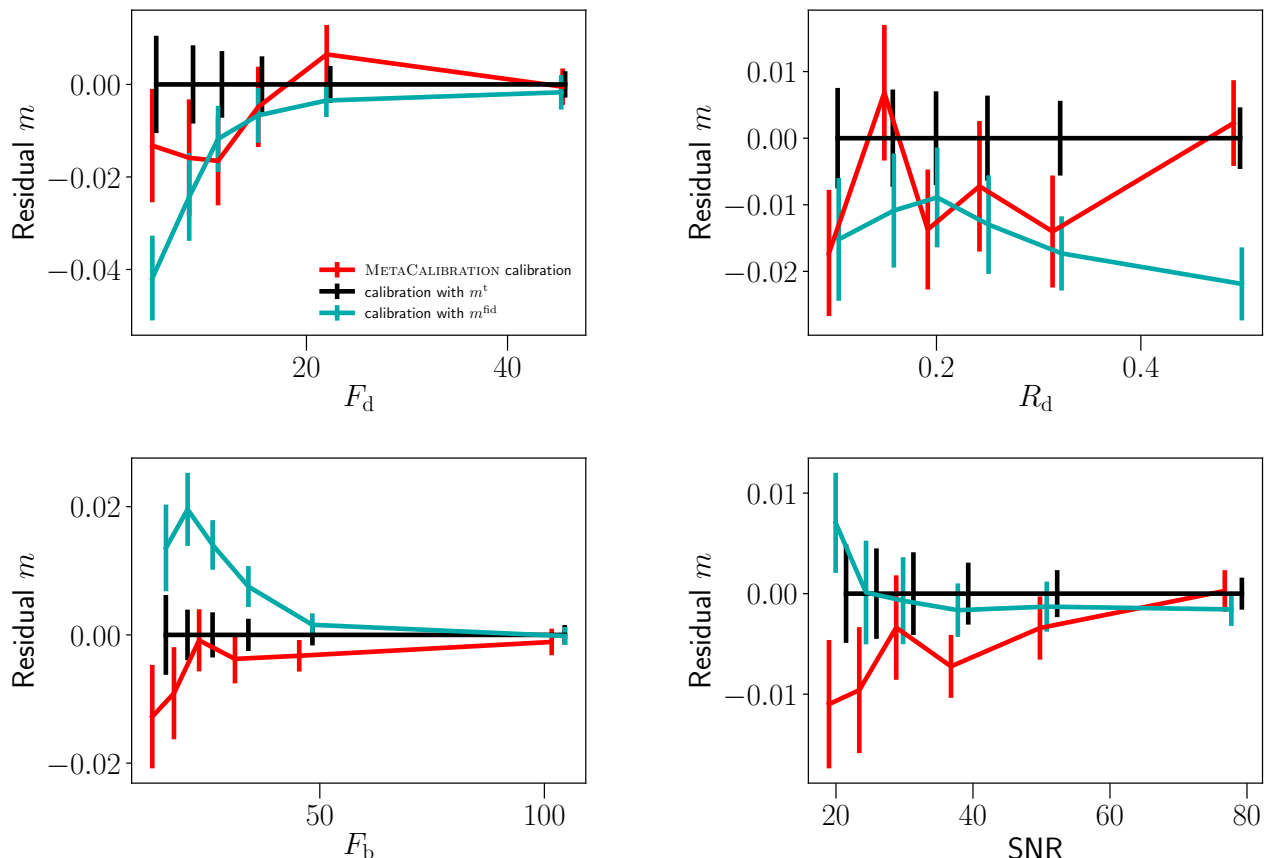


Fig. 6. Residual multiplicative shear bias as a function of input galaxy properties: disk flux (top left), disk half-light radius (top right), bulge flux (bottom left) and SNR (bottom right). Red lines show the calibration from METACALIBRATION. Black lines show the calibration using the true bias, and the cyan lines show the calibration using the bias estimation from NNSC.

to 4 percent for galaxies with a very dim disk. Remember that these are input properties from the simulations that have not been used for the training, so the performance of the calibration depends on the correlation between the measured properties used and these input properties. Since we use an estimation of the SNR in the training, the performance of the calibration is excellent even for galaxies with a very small SNR. On the other hand, galaxies with a low disk flux are not well characterized from the measured properties used in the training. They can be a combination of dim galaxies and galaxies with a very small disk fraction, and no measured properties aim to describe the morphology of the disk regardless of the contribution from the bulge. Because of this the NNSC performance on those galaxies is worse. Notice however that in real data applications we will never have access to this input information and the galaxies will always be selected from measured properties that can be included in the training set, so this problem will not appear on real data applications as it does here. Instead, this will produce selection effects that are discussed in Sect. 6.1.1.

5.5. Robustness with realistic images

The NNSC model has been trained with a specific set of image simulations, based on the CSC branch from GREAT3. To evaluate the potential impact of applying this model to real data with no further training, here we use the NNSC model that has been trained with the GREAT3-CSC images but applied to calibrate GREAT3-RSC images instead. In Fig. 7 we show the estimated bias (in green) compared to the real bias (in black) obtained from sheared versions of the images as in Pujol et al. (2019) using equations 3 and 4. The top panel shows the dependence of m on SNR, the bottom panels show the error on the estimation of m . We can see an error of up to 6 percent for the smallest SNR and ~ 1 percent for galaxies with $\text{SNR} > 20$. This indicates that the model trained on analytic, simpler galaxy images does not bring perfect estimations for realistic galaxy images, but it still obtains errors of ~ 1 percent for the majority of the cases.

Fig. 8 shows the residual bias after the calibration is applied to the GREAT3-RSC images, for both NNSC (cyan) and METACALIBRATION (red). Again, the training for the NNSC calibration used is the one from the CSC branch. The difference in the values of SNR with respect to pre-

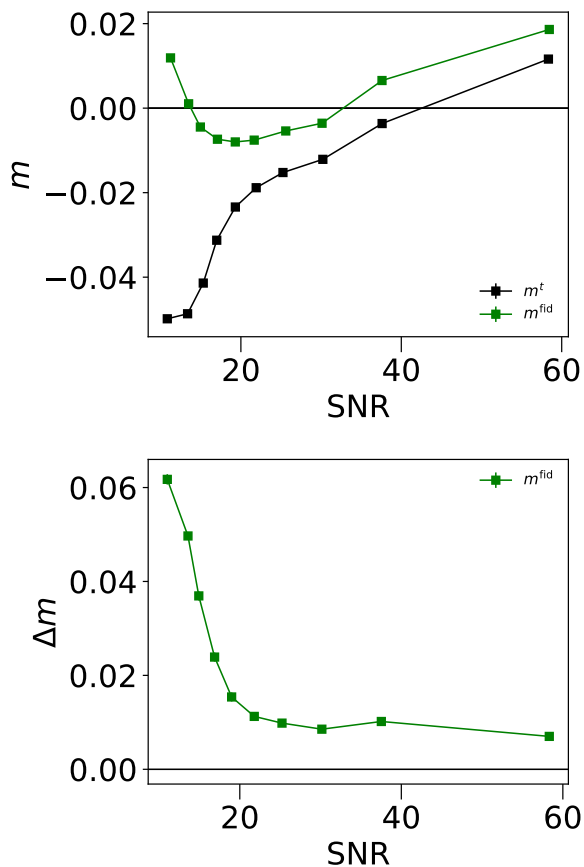


Fig. 7. Multiplicative bias predictions for GREAT3-RSC images as a function of SNR. Top panel shows the bias estimation from NNSC (green line) compared to the true bias (black line). The bottom panel shows the difference between the estimated and true bias as a function of SNR.

vious figures is that now we use the SNR estimation from KSB (for the rest we use the input parameter for GALSIM or the SNR from GFIT). For NNSC we can see a residual bias that decreases with SNR in consistency with the bias estimations from Fig. 7. It is not the scope of the paper to improve this calibration by applying a refinement on these images, since we want to show, on one side, the potential performance of the method (Sects. 5.1-5.3), and on the other side the impact of applying a crude calibration on a realistic data set for which the model has not been trained (this section). Otherwise, an easy improvement could be done with a refinement of the model on realistic galaxy images, or by identifying badly estimated objects (we have found that the major contribution of this error comes from objects whose shear responses have been estimated outside the range of values represented by the training, indicating a misrepresentation of those objects).

METACALIBRATION also shows a significant residual bias dependence on SNR for GREAT3-RSC images. Although the residual bias over all the population is very small and consistent with previous analyses (Huff & Mandelbaum 2017), the method shows a negative residual bias for small

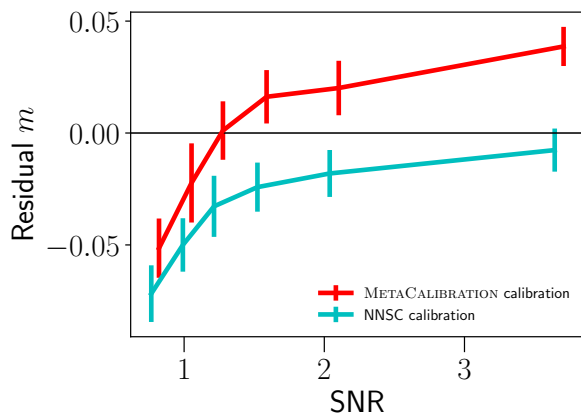


Fig. 8. Residual multiplicative bias after calibration for realistic images, using METACALIBRATION (red line) and the calibration from the bias estimation of NNSC (cyan line).

SNR galaxies and a positive one for high SNR. We have found this to be specific for the RSC images and this particular implementation. Differently than for CSC images, the estimated shear responses of METACALIBRATION show a small dependence on SNR. This is caused by some images that our KSB implementation interprets them to be small and a small window function is applied to them for the shape measurement. This produces a very similar calibration factor ($\sim 5\%$ positive) for all SNR values, producing a $\sim 5\%$ shift in the residual bias. We ignore the origin of this small sensitivity, and it can come from a combination of factors. First, RSC images are created from pixelated and noisy real images that have been deconvolved with their PSF and then applied a shear, making these images imperfect. On top of this, METACALIBRATION is ran, modifying again the images with a deconvolution, shearing, reconvolution and a noise addition. Finally, KSB estimates the optimal size of the window function to estimate the galaxy shape.

6. Discussion

6.1. Potential limitations and solutions for NNSC

6.1.1. Selection bias

The aim of this paper is to show the performance of NNSC to calibrate shear measurement bias. To this end, we have applied the following catalogue selection in order to have no selection bias in the data. For any galaxy whose detection or shape measurement has failed in any of the processes, this galaxy and all its shear versions are removed from the catalogue. This includes not only the shear versions simulated with GALSIM but also the images derived from the METACALIBRATION processing so that METACALIBRATION has no selection bias either. Also, when the data is split into bins of a measured variable, if a galaxy falls in different bins for different shear versions, all the shear versions are removed as well. With this, the selected data of our results

is identical for all shear versions, and selection bias is forced to be zero.

This procedure can be applied here for the purpose of presenting a method in simulations, but in real data selection effects are not avoidable and need to be calibrated. In particular, selection bias comes from the fact that the selection function depends on the shear, and is usually of the same order of magnitude than shear measurement bias (Fenech Conti et al. 2017; Mandelbaum et al. 2018a). METACALIBRATION takes into account the shear dependence of selection effects and also calibrates selection bias in a similar procedure than it does for measurement bias as described in Sheldon & Huff (2017). In Sheldon et al. (2019) they also explore a calibration of selection and measurement bias simultaneously in the presence of blended objects.

Analogously, NNSC can potentially be used to also calibrate selection bias. This would involve applying the same selection process to all galaxies independently of the shear and measuring the shear responses to this selection as described in Sheldon & Huff (2017) and in Sect. 7.2 of PKSB19:

$$\langle R_{\alpha\beta} \rangle \approx \frac{\langle e_{\alpha}^{\text{obs},+} \rangle - \langle e_{\alpha}^{\text{obs},-} \rangle}{2\Delta g_{\beta}}, \quad (8)$$

where the ellipticities are measured for the case with no shear and the + and - superscripts refer to the selection applied, corresponding to the catalogues obtained from the positive and negative shear versions respectively. A supervised training could be applied to learn the shear response on selection. This would involve adapting the method so that the selection is specified in the input data (e.g. with weights specifying the selection for each shear version). Then the cost function involves the average selection shear response over a subset of the catalogue, as:

$$C = \frac{1}{b_s} \sum_{i=0}^{b_s} \sum_{\alpha=1}^2 \sum_{\beta=1}^2 \left(\frac{w_i^+ e_{i,\alpha}^{\text{obs}} - w_i^- e_{i,\alpha}^{\text{obs}}}{2\Delta g_{\beta}} - R_{i,\alpha\beta}^e \right)^2, \quad (9)$$

where $w_i^{+,-}$ specifies the selection of the galaxy i for the cases with positive or negative shear (it can be a weight from 0 for undetected cases to 1 for detected cases with the full signal), $e_{i,\alpha}^{\text{obs}}$ is the observed ellipticity for the case with no shear and $R_{i,\alpha\beta}^e$ is the output estimated shear response of the training.

6.1.2. Model bias

For the results of our method in this paper, we used the same type of population for the training process than for the test and calibration. However, it is known that shear bias depends on the galaxy profile models (known as model bias). The images used in this paper consist of a mix of single Sérsic galaxies and galaxies with the sum of a bulge (de Vaucouleurs) and a disk (exponential). For the original training, test and calibration we use a population where 61% of the galaxies have single Sérsic profiles (this corresponds to the fraction in the whole set of images).

Here we quantify the impact of model bias on our method coming from these two different models by testing the performance of the method when different single Sérsic fractions are used for the training and the testing steps. In Fig. 9 we show the performance of the estimated multiplicative bias using different Sérsic population fractions for the training data as specified in the legends (m^{fid} corresponds to the original fraction of 61%, and m^t shows the true bias). The top panels show the results applied to the original population with a Sérsic fraction of 61%, in the middle panels we show the results on galaxies with a bulge and a disk (Sérsic fraction of 0%), and in the bottom panels we show the results applied to Sérsic galaxies (Sérsic fraction of 100%). The left panels show the bias dependence, and the differences with respect to the true are shown in the right panels.

In all the cases, we see that the best performance is obtained when the training population coincides with the test population. On the other hand, all the cases give different shear bias predictions for the different test populations. For example, the model trained with only Sérsic galaxies predicts $m \sim -0.06$ for the galaxies with a disk and a bulge and $m \sim -0.02$ for the single Sérsic galaxies. Although the true m changes a 5–6% between the two populations, training only with the single Sérsic population only gives $\sim 1\%$ error on the other population. In the opposite case, the model trained with disk and bulge galaxies predicts $m \sim 0.08$ for the same population and $m \sim 0.02 - 0.08$ for the single Sérsic population. This means that all the predictions are sensitive to the differences between the different populations, although model bias still remains nonzero, so we have captured only a part of the dependency of the bias on both SNR and type of galaxy. The red lines in the middle panel and the light green lines in the bottom panels can be seen as the extreme cases when the models have been trained with a completely different population, and they give a model bias of $\sim 1\%$ for bright galaxies. Possible ways to reduce this model bias could be a) training with more complex models, b) using more input measured complementary properties that can help to increase the sensitivity to more complex images, c) using convolutional neural networks (CNNs) to explore the information at the pixel level.

Finally, in Fig. 10 we show the same bias predictions but now applied to RSC images. This shows the impact of model bias when training different analytical models and applying them to realistic images. We see that the fiducial model gives better predictions on RSC images than the extreme cases where the training is only done with one galaxy model, at least for $\text{SNR} > 20$. A good performance is encouraging for the practical impact of model bias in real observations with our training, and using more sophisticated or realistic models for image simulations would potentially improve the performance, as discussed in Sect. 5.5.

6.2. Advantages of the NNSC method

In this paper we present NNSC as a new method for shear calibration. The method is different with respect to oth-

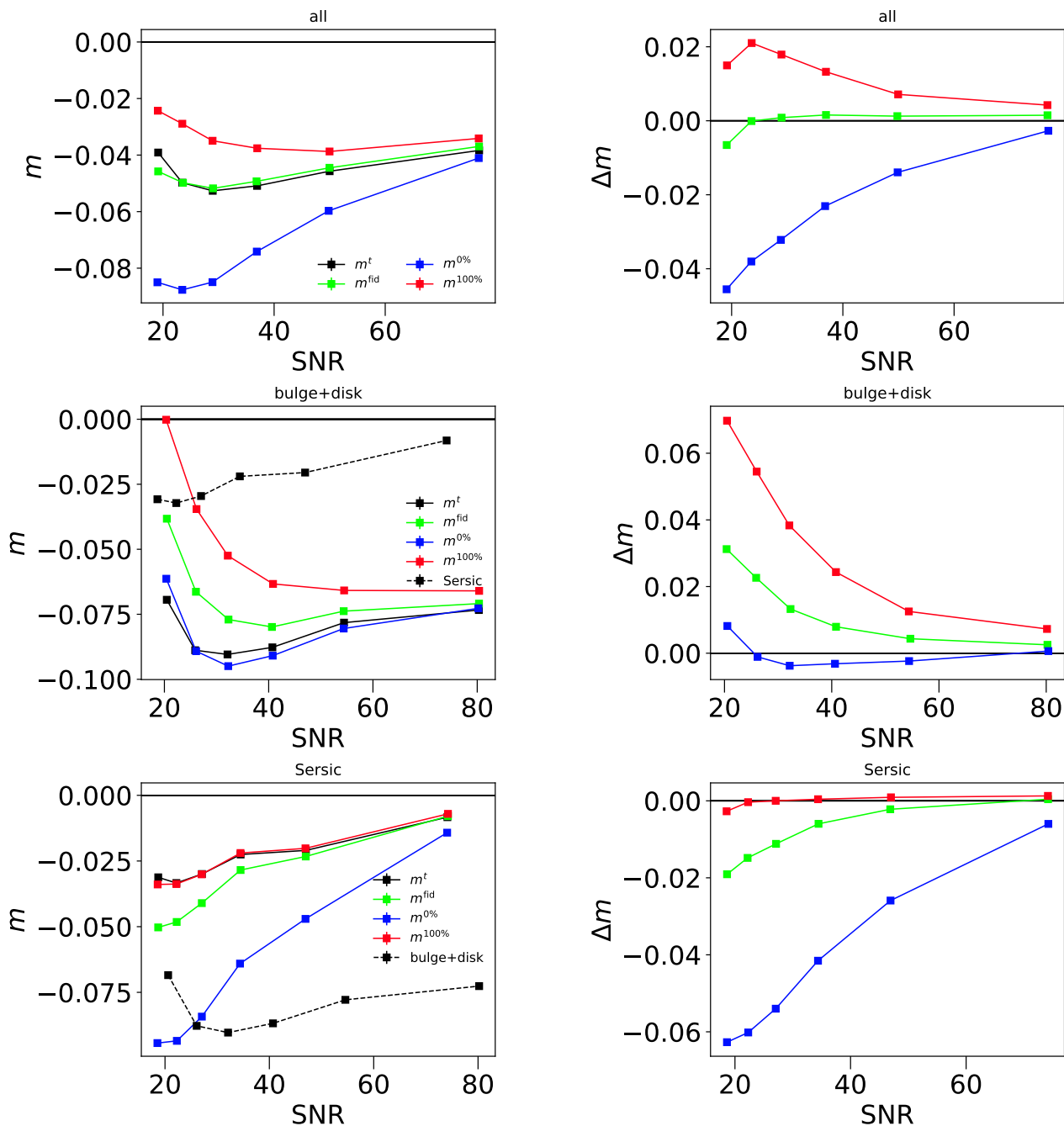


Fig. 9. Shear bias predictions using only single Sérsic (in red), only bulge+disk (in blue) or the real population (green) tested on the whole population (top), on only disk+bulge galaxies (middle) and on single Sérsic galaxies (bottom). Solid lines show the true bias of the populations, while the dashed black lines show the shear bias of the excluded population (the true bias for single Sérsic galaxies in the middle panels and for bulge+disk on the bottom).

ers such as METACALIBRATION, self-calibration methods, the commonly applied calibration from shear bias measurements in binned properties from simulations or other ML approaches. We do not claim one method or approach to be better than the other, but here we want to highlight several strengths of our method.

First, NNSC has the advantage that it can obtain a good performance in a matter of hours with a few thousand images, which is a very efficient ML approach for shear calibration. This is because, on one side, the input data is a reduced set of measured properties that significantly reduces the architecture dimensionality (compared to other ML approaches such as convolutional neural networks), and

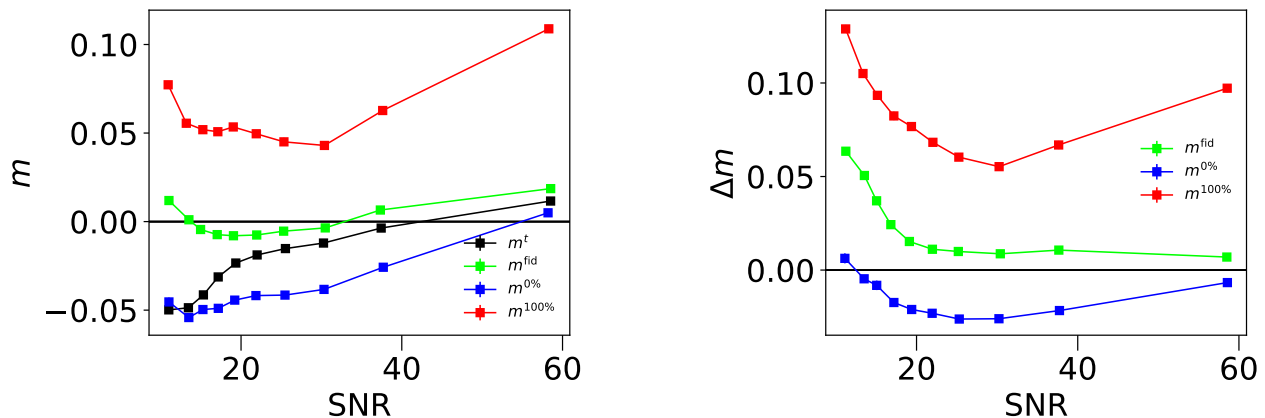


Fig. 10. The same as in Fig. 9 but applied to the realistic RSC images.

on the other side by focusing on minimizing the error on the estimated individual shear response we avoid the shape noise contribution of the intrinsic ellipticity (see PKS19 for a detailed discussion on this contribution). It could also be possible to build an estimate of the shear bias straight from the galaxy and PSF images (e.g. from convolutional neural network), but this would require a much more complex network architecture (e.g. accounting for the effect of the PSF, galaxy morphology, etc.). Learning from image properties already reduces the complexity of the images, without losing too much information about the shear bias.

As an example of a ML approach, Tewes et al. (2019) minimizes the residual bias over the average measured ellipticities so that the output is an unbiased estimator of shear. Because of the intrinsic ellipticity contribution, the method requires a very large catalogue ($10^6 - 10^7$ objects) and uses a batch size of 500,000 objects (distributed so that the intrinsic ellipticity cancels out) to ensure that in each minimization step the shape noise from the intrinsic ellipticity is small. One suggestion to improve the computational performance of Tewes et al. (2019) would be to minimize the individual responses (using sheared versions of the same images as in this paper and in PKS19) instead of the residual bias over average ellipticities.

In another approach, Gruen et al. (2010) minimizes shear bias for a KSB estimator by training the ellipticity measurement errors using the original measurements from KSB the flux measured from SExtractor and some tensors involved in the shape measurement process. The approach is similar to ours in the sense that they consider a set of properties to estimate errors on the shape measurements, but the fact that our method directly estimates the shear response avoids shape noise. As in Tewes et al. (2019), Gruen et al. (2010) uses $\sim 10^7$ objects for the training sets.

Another potential of the NNSC method is that it can be easily implemented for any survey for which we have image simulations (something that is required for a good validation of the survey exploitation). To apply NNSC we only need to produce copies of the same image simulations with different shear values applied, so that we can obtain individual shear responses. The set of measured properties

to be used for the training is arbitrary and can be chosen according to the interests and the pipeline output of the surveys. Even a simple application using a few properties of interest will be already an improvement with respect to common calibrations obtained from shear bias measurements in simulations as a function of two properties only. Moreover, as mentioned in Sect. 6.1.1, the method can be extended to also calibrate selection bias.

Finally, the method allows us to use as input a large set of measured properties. When properly trained, this allows the calibration to be more robust with respect to the particular population distribution of the training with respect to the real data. If the bias dependencies on many properties are correctly learnt, the particular distribution of the population over these properties should not affect the performance of the calibration (provided that no other unaccounted properties affect shear bias and the simulated population is representative of the real data).

6.3. Importance of using complementary methods

In this paper we have used two different methods (METACALIBRATION and NNSC) and analysed their performances in image simulations. Both methods give good performances, and they are complementary because they do not share the same systematics. Different implementations of the METACALIBRATION pipeline, as well as using other shape estimators, might improve or be better adapted to the particular data. As for our model, the scope of this paper is not to show the best implementation of METACALIBRATION for this particular data, but to include it to compare NNSC with a reference of the state-of-the-art.

Given the complementarity of the two models, using both for the same scientific analyses is a more suited approach to ensure the robustness of the results. For this reason we encourage to include at least two independent shear measurements and calibration methods for scientific analyses on galaxy surveys, as it is done in DES (Jarvis et al. 2016; Zuntz et al. 2018). This allows us to better identify systematics from the discrepancies between the methods that otherwise they might be missed. At the same time,

consistent results from two different and independent methods always give robustness to the scientific results, a crucial aspect for future precision cosmology. The combination of NNSC and METACALIBRATION brings a good complementarity since it uses a ML approach based on measurements from image simulations and a method that is independent on image simulations but limited by other numerical processes.

7. Conclusions

ML is a promising and exploiting tool for astronomical analyses due to its power to characterise complex systems from large data sets. It is then specially suited for shear calibration, where many systematics complicate the behaviour of shear bias and its calibration.

In this paper we present a new shear calibration method based on machine learning (ML) that we call Neural Network Shear Correction (NNSC). We have also made the code publicly available. The method is based on galaxy image simulations that are produced several times with different shear versions but preserving the rest of the conditions. With this, we obtain the individual shear response of the objects that serves us for a supervised ML algorithm to estimate the shear responses of objects from an arbitrarily large set of measured properties (such as SNR, size, flux, ellipticity, PSF properties, etc.) through a regression approach.

This ML approach allows us to characterize the complexity of shear bias dependencies as a function of many properties, a complexity that we explore in Pujol et al. (2017). The advantage of ML is that it is a specially suited approach to reproduce very complex systems so that we can include a large set of properties for which shear bias can depend on. With them, the algorithm identifies the contribution of each of the properties and their correlations to estimate shear bias. With the individual shear bias estimations of galaxies we can then apply a shear calibration from the average statistics of shape measurements as in many other shear calibration approaches.

We have used image simulations based on the GREAT3 (Mandelbaum et al. 2014) control-space-constant branch to explore the method, apply the training algorithm of NNSC and evaluate its performance through tests and validations. We have obtained a performance beyond Euclid requirements ($\Delta m_1 = (4.9 \pm 1.1) \times 10^{-4}$, $\Delta m_2 = (0.0 \pm 1.1) \times 10^{-4}$, $\Delta c_1 = (-3.1 \pm 0.7) \times 10^{-4}$ and $\Delta c_2 = (1.6 \pm 0.7) \times 10^{-4}$) for the estimations of the average shear biases, and we have shown shear bias dependencies on one and two properties below the one percent error. This performance is achieved with only ~ 15 CPU hours of training using 128,000 objects, which is a very cheap and fast training compared to common ML approaches (the method from Tewes et al. (2019) takes around 2 CPU-days with $10^6 - 10^7$ objects). This makes the NNSC approach not only to have a high potential, but also to be very easy to apply to galaxy surveys, since it only requires different shear versions of the same image simulations and low computational and storage capacities.

We have compared the residual bias after calibration as a function of several input properties with the state-of-the-art method METACALIBRATION, giving similar performances and showing different dependencies due to the differences between the approaches and their systematics.

We have quantified the impact of model bias by applying the calibration to different galaxy morphologies than those used for the training. We have found errors of a few percent in some extreme cases that could be improved by refining the training with a more proper or sophisticated data set. Although it is not developed in this paper, the method can be easily adapted to also learn selection bias and calibrate for it just by adding information about the data selection as input data for the training and applying small changes in the cost function.

Our method is an implementation of ML based on a simple DNN architecture leading to fast calibration that can be easily applied to weak lensing analyses on current and future galaxy surveys and can be a good complementary method to combine with other with state-of-the-art approaches and gain sensibility to systematics and robustness to the science.

Acknowledgements

AP, FS and JB acknowledge support from a European Research Council Starting Grant (LENA-678282). This work has been supported by MINECO grants AYA2015-71825, PGC2018-102021-B-100 and Juan de la Cierva fellowship, LACEGAL and EWC Marie Skłodowska-Curie grant No 734374 and no.776247 with ERDF funds from the EU Horizon 2020 Programme. IEEC is partially funded by the CERCA program of the Generalitat de Catalunya.

References

- Akeson, R., Armus, L., Bachelet, E., et al. 2019, arXiv e-prints, arXiv:1902.05569
- Bernstein, G. M. 2010, MNRAS, 406, 2793
- Bridle, S., Balan, S. T., Bethge, M., et al. 2010, MNRAS, 405, 2044
- Bridle, S., Shave-Taylor, J., Amara, A., et al. 2009, Annals of Applied Statistics, 3, 6
- Clampitt, J., Sánchez, C., Kwan, J., et al. 2017, MNRAS, 465, 4204
- Fenech Conti, I., Herbonnet, R., Hoekstra, H., et al. 2017, MNRAS, 467, 1627
- Gruen, D., Seitz, S., Koppenhoefer, J., & Riffeser, A. 2010, ApJ, 720, 639
- Hall, A. & Taylor, A. 2017, MNRAS, 468, 346
- Hildebrandt, H., Viola, M., Heymans, C., et al. 2017, MNRAS, 465, 1454
- Hoekstra, H., Herbonnet, R., Muzzin, A., et al. 2015, MNRAS, 449, 685
- Hoekstra, H., Viola, M., & Herbonnet, R. 2017, MNRAS, 468, 3295
- Huff, E. & Mandelbaum, R. 2017, ArXiv e-prints [arXiv:1702.02600]
- Jarvis, M., Sheldon, E., Zuntz, J., et al. 2016, MNRAS, 460, 2245
- Kacprzak, T., Bridle, S., Rowe, B., et al. 2014, MNRAS, 441, 2528
- Kacprzak, T., Zuntz, J., Rowe, B., et al. 2012, MNRAS, 427, 2711
- Kaiser, N., Squires, G., & Broadhurst, T. 1995, ApJ, 449, 460
- Kannawadi, A., Hoekstra, H., Miller, L., et al. 2019, A&A, 624, A92
- Kitching, T., Balan, S., Bernstein, G., et al. 2010, ArXiv e-prints [arXiv:1009.0779]
- Kitching, T. D., Balan, S. T., Bridle, S., et al. 2012, MNRAS, 423, 3163
- Kitching, T. D., Rowe, B., Gill, M., et al. 2013, ApJS, 205, 12

- Laureijs, R., Amiaux, J., Arduini, S., et al. 2011, ArXiv e-prints [arXiv:1110.3193]
- LSST Science Collaboration, Abell, P. A., Allison, J., et al. 2009, ArXiv e-prints [arXiv:0912.0201]
- Mandelbaum, R. 2018, ARA&A, 56, 393
- Mandelbaum, R., Lanusse, F., Leauthaud, A., et al. 2018a, MNRAS, 481, 3170
- Mandelbaum, R., Miyatake, H., Hamana, T., et al. 2018b, PASJ, 70, S25
- Mandelbaum, R., Rowe, B., Armstrong, R., et al. 2015, MNRAS, 450, 2963
- Mandelbaum, R., Rowe, B., Bosch, J., et al. 2014, ApJS, 212, 5
- Mandelbaum, R., Slosar, A., Baldauf, T., et al. 2013, MNRAS, 432, 1544
- Massey, R., Heymans, C., Bergé, J., et al. 2007, MNRAS, 376, 13
- Massey, R., Hoekstra, H., Kitching, T., et al. 2013, MNRAS, 429, 661
- Melchior, P. & Viola, M. 2012, MNRAS, 424, 2757
- Pujol, A., Kilbinger, M., Sureau, F., & Bobin, J. 2019, A&A, 621, A2
- Pujol, A., Sureau, F., Bobin, J., et al. 2017, ArXiv e-prints [arXiv:1707.01285]
- Refregier, A., Kacprzak, T., Amara, A., Bridle, S., & Rowe, B. 2012, MNRAS, 425, 1951
- Rowe, B. T. P., Jarvis, M., Mandelbaum, R., et al. 2015, Astronomy and Computing, 10, 121
- Sheldon, E. S., Becker, M. R., MacCrann, N., & Jarvis, M. 2019, arXiv e-prints, arXiv:1911.02505
- Sheldon, E. S. & Huff, E. M. 2017, ApJ, 841, 24
- Taylor, A. N. & Kitching, T. D. 2016, ArXiv e-prints [arXiv:1605.09130]
- Tessore, N. & Bridle, S. 2019, New A, 69, 58
- Tewes, M., Kuntzer, T., Nakajima, R., et al. 2019, A&A, 621, A36
- Voigt, L. M. & Bridle, S. L. 2010, MNRAS, 404, 458
- Zhang, J. & Komatsu, E. 2011, MNRAS, 414, 1047
- Zuntz, J., Kacprzak, T., Voigt, L., et al. 2013, MNRAS, 434, 1604
- Zuntz, J., Sheldon, E., Samuroff, S., et al. 2018, MNRAS, 481, 1149

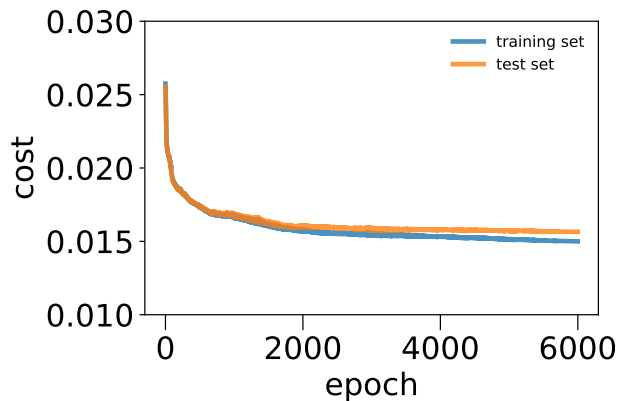


Fig. A.1. Evolution of the cost function for the training and the test sets during the training on the fiducial implementation of NNSC.

Appendix A: Details on training

In this section we describe the training procedure and the architecture, cost function and hyperparameters implemented for the results shown in this paper. This configuration has been chosen according to the performances found during the optimization process. Even if these optimization parameters could be further studied and optimized, we already obtained competitive results with the procedure and the optimization tests described below

Our configuration consists on a DNN with 4 hidden layers of 30 units per layer. The input consists of the 27 measured properties as described before, and the output consists on the 4 shear bias components.

First of all, we apply a whitening with principal component analysis (PCA) to the input data in order to decorrelate the 27 properties and we normalize them to be between 0 and 1. This procedure aims at avoiding some properties or information to dominate their contribution due to their value ranges or correlations.

Here we remind the cost function C that minimizes the χ^2 on the estimated shear biases:

$$C = \frac{1}{b_s} \sum_{i=0}^{b_s} \sum_{\alpha=1}^2 (m_{i,\alpha}^t - m_{i,\alpha}^e)^2 + (c_{i,\alpha}^t - c_{i,\alpha}^e)^2, \quad (\text{A.1})$$

where m_{α}^t , c_{α}^t and m_{α}^e , c_{α}^e are the true and estimated α th component shear multiplicative and additive bias, respectively, and b_s is the batch size. Given that usually $m_{i,\alpha} \gg c_{i,\alpha}$, the contribution of $m_{i,\alpha}$ in the current approach is dominating the minimization process, but extra weights can be applied to some biases if we want to increase the performance of the estimation of these biases differently. Here we include the four bias components in the cost function to estimate them simultaneously, but separate trainings for each of the components can also be done. Doing a separate trainings for each of the components might allow using simpler architecture and a faster learning, but it would miss the correlation between the components on the model learned.

We have constrained the hyperparameters of the algorithm (contamination level, number of training objects, number of epochs, batch size, learning rate and learning decay rate) by analyzing the performance and convergence on a wide hyperparameter space, choosing the final hyperparameter set from the best cases that we have found avoiding overfitting according to the cost function values of the training and test sets (see Fig. A.1 for the evolution of the cost function during the training of the fiducial example). For this, we have evaluated the cost function in the training and the test sets to ensure that, on one side, the costs converge during the training, and on another side, the cost in the training set is not significantly smaller than the cost in the test set, which would be a symptom of overfitting. In some cases, the test cost has been found to be smaller than the training set. These cases have also been discarded for this accidental overfitting.

In Fig. A.2 we show the performance of the shear bias estimations for different hyperparameters of the ML optimization. Left panels show the shear bias dependence as a function of SNR for the true multiplicative bias (black lines) and the estimated biases (colour lines). The right panels show the difference between the estimated and true bias as a function of SNR.

In the top panel we show the performance for different number of objects used in the training set, going from 16,000 to 256,000 objects (the fiducial case is done with 128,000 objects). We see that using more objects improves the performance, reaching some plateau for more than 50,000 objects. Notice that this is a very small number of objects compared with most of the shear calibration approaches (Zuntz et al. 2018; Tewes et al. 2019; Kannawadi et al. 2019).

The middle panels show the performance as a function of the number of epochs used in the training (with 6,000 epochs for the fiducial case). In this case, we see that the training converges for more than 6000 epochs. For our final case we use 6000 epochs, which takes around 15 CPU hours of training, but we note that similar results are obtained with longer trainings. This shows that our method has a very fast training compared to other ML approaches.

In the bottom panels we compare the performance using different architectures. Our final case uses 4 hidden layers with 30 nodes in each layer, but here we compare it with a case of a narrower architecture (with 4 hidden layers with 30, 20, 10 and 10 nodes), a shallow one (with 2 hidden layers of 90 and 10 units) and a larger one (with 4 hidden layers of 50 nodes each). The performances as a function of SNR are very similar, with no obvious conclusion about which architecture is giving better predictions. However, in Fig.A.3 we can see the interest of using a wider and deeper architecture. In the top left panel, we show the true m_1 as a function of two properties (the two ellipticity components measured by KSB). The other panels show the difference between the estimated and the true m_1 for the large architecture (top right), the shallow (bottom left) and the narrow (bottom right) architectures. We see that the narrow and shallow architectures are not able to capture all the complexity of the 2d-dependence as efficiently as our

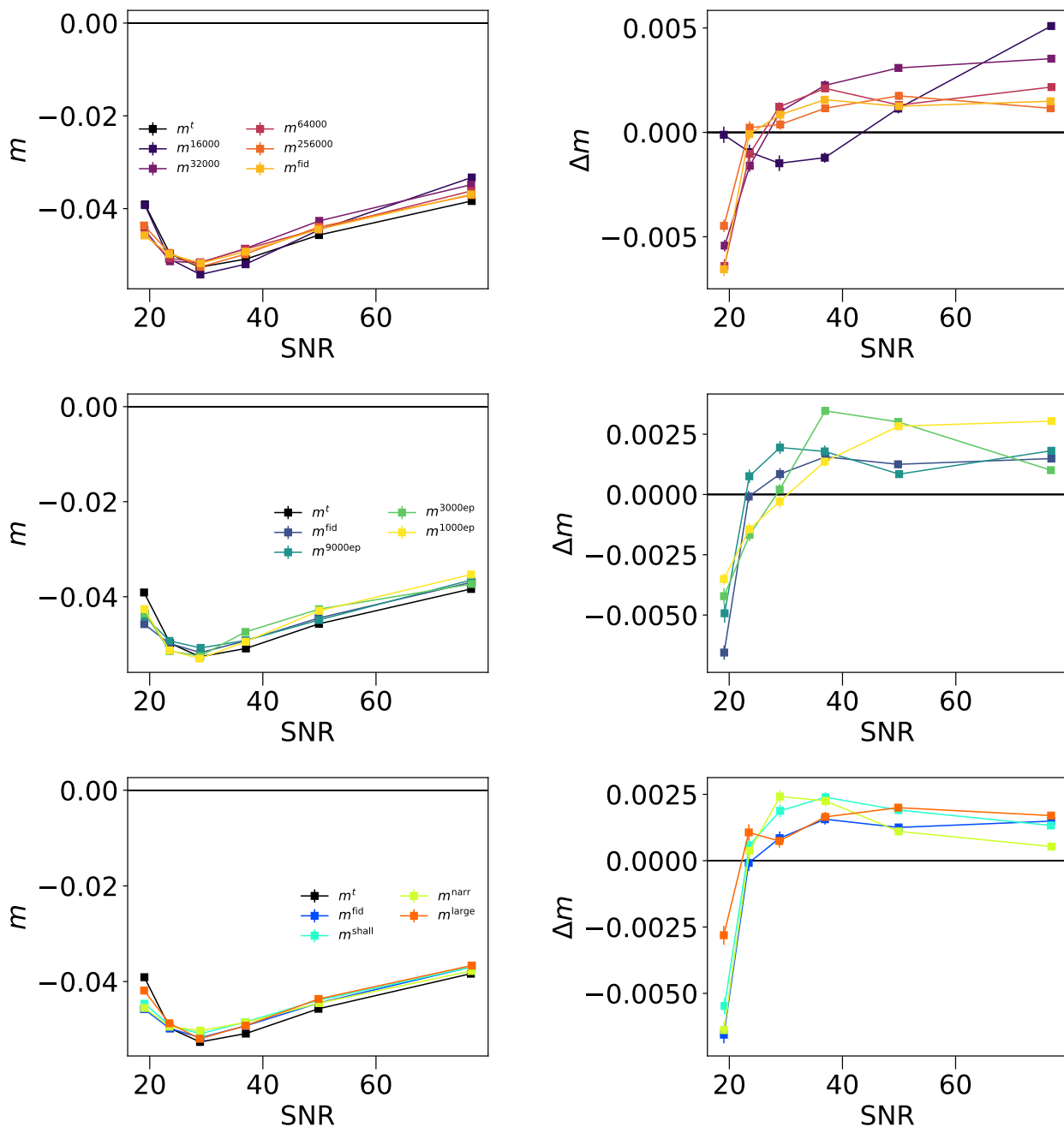


Fig. A.2. Comparison of estimated multiplicative shear bias m_1 (left) and its error Δm_1 (right) as a function of SNR for different machine-learning hyperparameters. The top panels show the performance for different numbers of objects used in the training, from 10,000 to 400,000. The middle panels show the performances for the chosen architecture for different number of epochs, from 1,000 to 9,000. The bottom panels show the performance of different architectures. The chosen one, shown in blue, corresponds to 4 hidden layers of 30 nodes each. The shallow architecture, shown in green, has only 2 hidden layers of 30 nodes. The Narrow architecture, shown in orange, corresponds to 4 hidden layers of 30, 20, 10 and 10 nodes.

fiducial architecture, a proof that a wide and deep neural network allows us to better capture the complexity of the system. Although not shown here, the larger architecture gives very similar performances than the fiducial one, and in fact the performance is worse for the same training time. This indicates that the largest architecture does not help to

improve the performance and loses efficiency of the training, and for this reason we kept the four hidden layers of 30 nodes as the fiducial model for the purpose of this paper.

For the rest of the hyperparameters we mention that we did not find a strong dependence on the batch size, showing good performance between 16 and 256 (32 has been finally

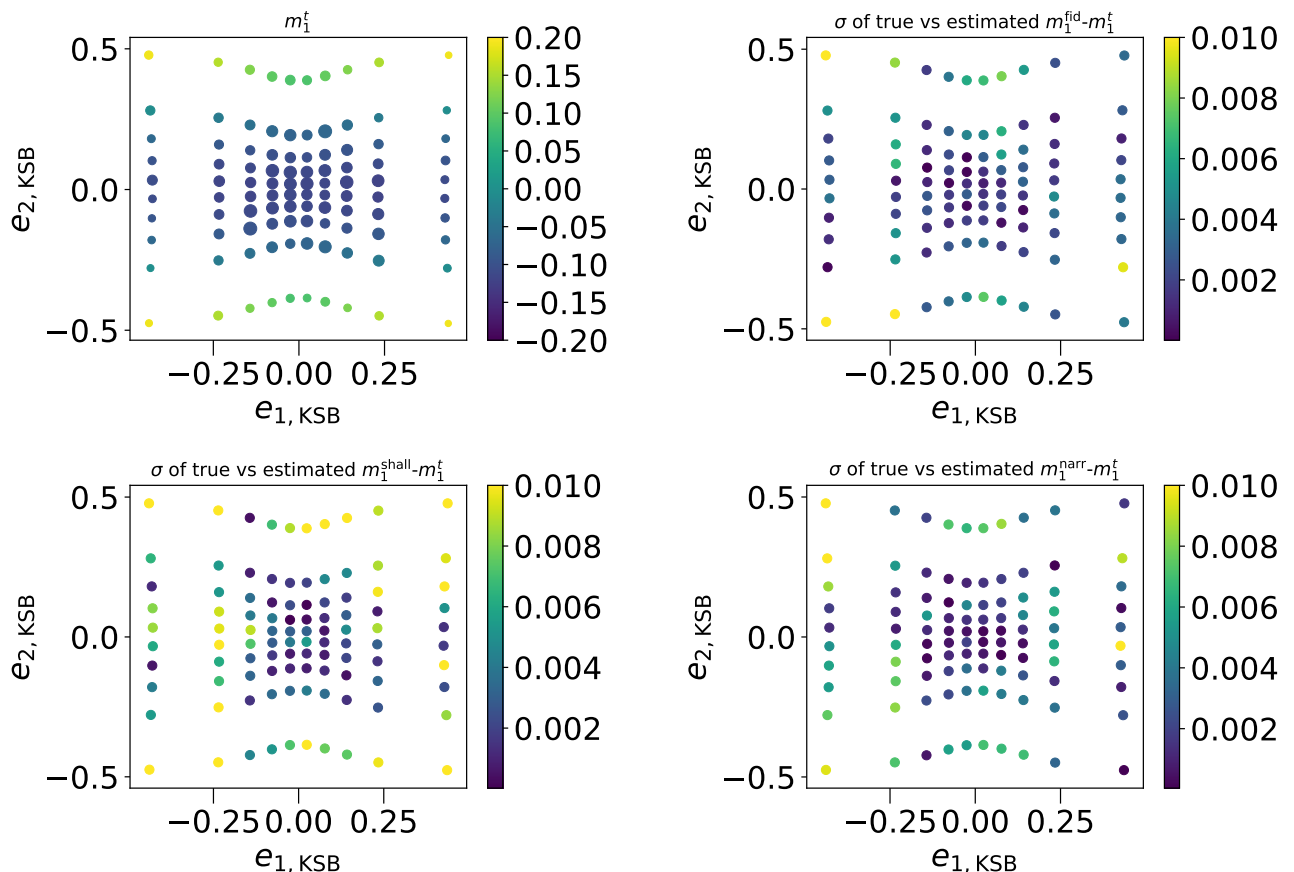


Fig. A.3. Comparison of estimated multiplicative shear bias m_1 as a function of galaxy measured ellipticities. The top left panel shows the true values of m_1 , and the rest of the panels show the difference between the estimated and the true for the fiducial architecture (top right), the shallow architecture (bottom left) and the narrow one (bottom right).

chosen), and we found that adding no noise contamination on the input data was optimal for the performance. About the activation function of the layers, we use a weakly relu function for the nodes. We have found similar performances using using tanh functions or combinations of both, but with a significantly slower convergence. The results shown in the paper for the chosen model are obtained with ≈ 15 CPU hours.

Appendix B: Metacalibration

The calibration method METACALIBRATION has been presented in Huff & Mandelbaum (2017) and Sheldon & Huff (2017), with a publicly available implementation². It has been tested on simulations and applied to the Dark Energy Survey (DES) Y1 data (Zuntz et al. 2018), showing a very good performance. In this paper we use this as a reference state-of-the-art calibration method for comparison with our new approach. Here we briefly describe the idea of this method and refer to Huff & Mandelbaum (2017) and Sheldon & Huff (2017) for more details.

² <https://github.com/esheldon/ngmix/wiki/Metacalibration>

METACALIBRATION is based on measuring the shear response of the individual galaxy images without any need of image simulations. To do so, METACALIBRATION uses the original real image to generate sheared versions of it. With these sheared versions, the shear response is obtained using Eq. 2 as in our method. The shear calibration is then applied to the data using the mean of these individual shear responses and their propagation through the statistics of interest.

To generate the sheared versions of the original image, METACALIBRATION first deconvolves the image with the PSF (that is assumed to be perfectly known). Then, the shear distortion is applied, and the image is reconvolved with a slightly larger PSF. As this process induces correlated sheared noise, a noise image following the same procedure but with opposite sign shear is also added to reduce the impact of this correlated shear on the shear response. The final noise realizations can be significantly different than the original one, which can have an impact on the shear response. Because of this, a non-sheared new image is also generated via the same process. It is this new image on which shear is measured and calibrated for science analyses. In addition, the additive bias can be measured, using Eq. 18 from Huff & Mandelbaum (2017), and the shear response

coming from selection biases can be estimated (Sheldon & Huff 2017).

METACALIBRATION has the advantage that no image simulations for the calibration are required (although its performance can only be tested in simulations). On the other hand, the method depends on the numerical processes involving deconvolution, reconvolution, and the treatment of noise.

METACALIBRATION allows for different implementations regarding the characterization of the PSF, including a Gaussian parameter fitting of the PSF (so that a combination of Gaussian profiles is used as the PSF), a symmetrization (where three different rotations of the PSF are stacked to avoid a contribution of its ellipticity) and using the true PSF directly. In our case we use the true PSF, but we have found very similar results using the symmetrization. Also, METACALIBRATION can be applied for any shape measurement algorithm, for which the method calibrates its shear bias. In our case, we use METACALIBRATION to calibrate the KSB measurements from the software SHAPELENS.